JACS
JOURNAL OF THE AMERICAN CHEMICAL SOCIETY

Article

pubs.acs.org/JACS

Impact of Alkyl Spacer Length on Aggregation Pathways in Kinetically Controlled Supramolecular Polymerization

Soichiro Ogi, Vladimir Stepanenko, Johannes Thein, and Frank Würthner*

Universität Würzburg, Institut für Organische Chemie and Center for Nanosystems Chemistry, Am Hubland, 97074 Würzburg, Germany

Supporting Information

ABSTRACT: We have investigated the kinetic and thermodynamic supramolecular polymerizations of a series of amide-functionalized perylene bisimide (PBI) organogelator molecules bearing alkyl spacers of varied lengths (ethylene to pentylene chains, **PBI-1-C2** to **PBI-1-C5**) between the amide and PBI imide groups. These amide-functionalized PBIs form one-dimensional fibrous nanostructures as the thermodynamically favored states in solvents of low polarity. Our in-depth studies revealed, however, that the kinetic behavior of their supramolecular polymerization is dependent on the spacer length. Propylene- and pentylene-tethered PBIs follow a similar polymerization process as previously observed for the ethylene-tethered PBI. Thus, the monomers of these PBIs are kinetically trapped in conformationally restricted states through intramolecular hydrogen bonding between the amide and imide groups. In contrast, the intramolecularly hydrogen-bonded monomers of butylene-tethered PBI spontaneously self-assemble into nanoparticles, which constitute an off-pathway aggregate state with regard to the thermodynamically stable fibrous supramolecular polymers obtained. Thus, for this class of π-conjugated system, an unprecedented off-pathway aggregate with high kinetic stability could be realized for the first time by introducing an alkyl linker of optimum length (C4 chain) between the amide and imide groups. Our current system with an energy landscape of two competing nucleated aggregation pathways is applicable to the kinetic control over the supramolecular polymerization by the seeding approach.

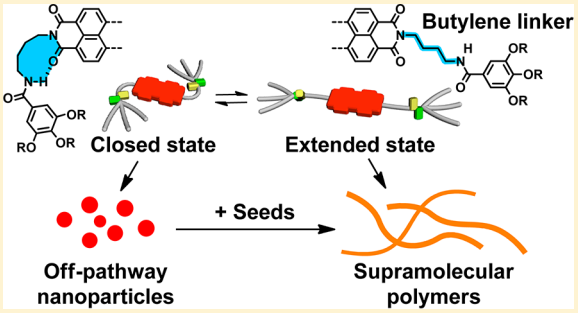

INTRODUCTION

Supramolecular polymerization currently attracts particular attention as a methodology to exploit the potential for the organization of π-conjugated molecules into novel one-dimensional architectures with controlled average size, polydispersity, ordering, and homogeneity.[1] Such structural parameters have recently been shown to be controlled precisely by kinetics,[2,3] as distinct from thermodynamics that have been considered commonly in the development of supramolecular polymers.[4] A promising method to get control over kinetics of one-dimensional aggregation processes is living supramolecular polymerization,[5−7] which is designed by seed-induced growth of monomeric species.[8−10] In the seeding approach, the initiation step of supramolecular polymerization is kinetically regulated by external addition of seeds. The seed bearing preorganized active sites (e.g., termini of short nanofibers) is a suitable supramolecular initiator to associate efficiently with monomeric species and grow into supramolecular polymers in a living manner. Accordingly, supramolecular polymers can be synthesized with narrow polydispersity.[5] In addition, the size of supramolecular polymers, which is one of the fundamental structural parameters, is controllable by adjusting the mixing ratio of monomeric species and seeds.[5] However, such seeded supramolecular polymerization competes with a self-assembly process, where the initial binding step (nucleation) occurs spontaneously, providing supramolecular polymers with a broad size distribution.[4]

To retard the spontaneous self-assembly, it is essential to construct a far-from-equilibrium condition, where monomeric species are kinetically trapped in an inactive state.[11] In this regard, the design of an additional noncovalent interaction such as intramolecular hydrogen bonding is an appropriate approach to create an aggregation-incompetent conformation.[12,13] For example, Miyajima, Aida, and co-workers have reported that a spontaneous polymerization of a bowl-shaped corannulene derivative bearing five amide groups is absent in nonpolar solvent due to trapping of the monomeric state in an intramolecular hydrogen-bonded conformation.[12] Similarly, we have previously shown that a planar perylene bisimide (PBI) derivative containing amide groups at the imide positions is kinetically inactivated in the supramolecular polymerization process because the amide hydrogens are intramolecularly hydrogen-bonded to the imide carbonyl oxygens of the PBI (**PBI-1-C2** in Figure 1).[13] According to the pioneering work of Gellman et al. and Nowick et al. on bis-amides and bis-ureas, the equilibrium for the formation of an intramolecular hydrogen bond is strongly affected by the chosen length of

Received: November 7, 2015
Published: December 23, 2015

DOI: 10.1021/jacs.5b11674
J. Am. Chem. Soc. 2016, 138, 670−678

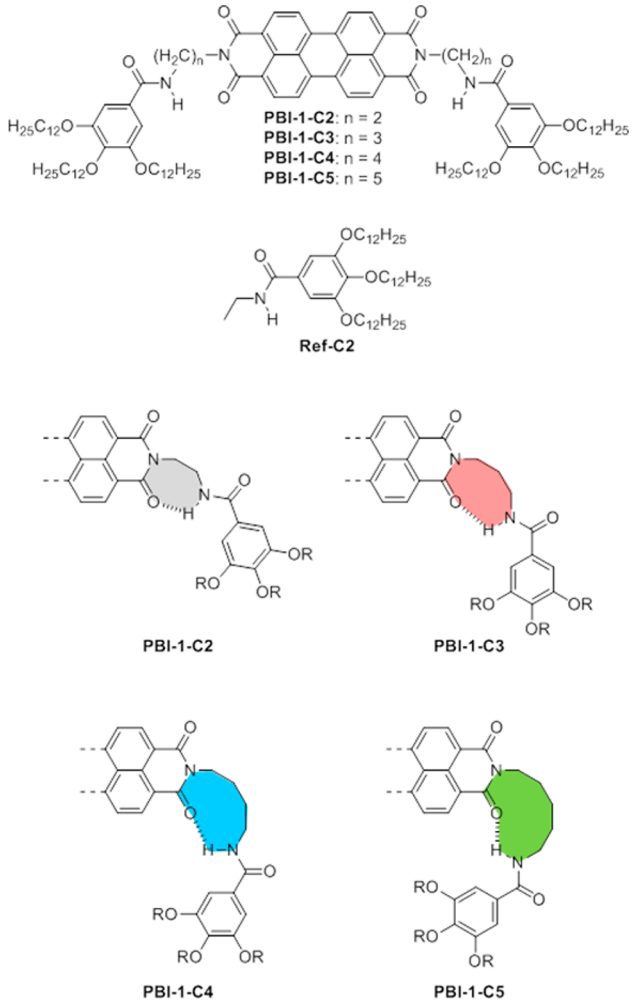

Figure 1. Chemical structures of PBI derivatives **PBI-1-C2** to **PBI-1-C5** with different lengths of alkyl linkers between imide and amide groups and reference compound **ref-C2**, and an illustration of the conceivable conformations of intramolecularly hydrogen-bonded PBI derivatives (half of each of these symmetrical molecules is shown, and the dodecyl groups are denoted as R).

alkyl spacer between two amide or two urea groups.[14,15] Thus, we hypothesized that the kinetic stability of the intramolecular hydrogen-bonded (trapped) state in our PBI system should be controllable by changing the length of alkyl spacer between the amide and imide nitrogen atoms. Such structural modification would result in control over the balance between the inactivation and polymerization pathways, leading to programmable supramolecular polymerization.[2b] To verify this intriguing concept based on molecular design, we have investigated the kinetic as well as thermodynamic self-assembly behavior of a series of amide-functionalized PBI derivatives **PBI-1-C2** to **PBI-1-C5** with varied alkyl spacers (ethylene to pentylene chains) between the amide group and PBI core (Figure 1).

Our detailed studies revealed that the competing off-pathway aggregation[16] and thermodynamically favored supramolecular polymerization can indeed be modulated by alkyl spacer length. Importantly, these two pathways can be described by the cooperative nucleation-elongation model but are directed from two different monomeric species, namely the intramolecularly hydrogen-bonded and non-hydrogen-bonded extended monomers. The large energy barrier provided by the formation of the off-pathway aggregate enables efficient inhibition of the spontaneous supramolecular polymerization in low polarity solvents at higher concentrations and thus facilitates kinetic regulation of the initiation step in supramolecular polymerization by the seeding approach.

RESULTS AND DISCUSSION

Synthesis and Molecular Properties. By following the reported method for the synthesis of **PBI-1-C2**,[17] the new PBI derivatives applied in this study were synthesized through imidization of perylene-3,4:9,10-tetracarboxylic acid bisanhydride with 3,4,5-tris(dodecyloxy)benzoic acid aminopropylamide for **PBI-1-C3**, 3,4,5-tris(dodecyloxy)-benzoic acid aminobutylamide for **PBI-1-C4**, and 3,4,5-tris(dodecyloxy)benzoic acid aminopentylamide for **PBI-1-C5** in imidazole using $Zn(OAc)_2$ as a catalyst and isolated as red solids in the yields of 75%, 76%, and 75%, respectively (for structures see Figure 1). Benzamide **ref-C2** was synthesized by the reaction of 3,4,5-tris(dodecyloxy)benzoic acid with thionyl chloride and subsequent amidation with ethylamine and used as a reference compound because this amide cannot form an intramolecular hydrogen bond. The synthesis details and characterization data of all new compounds are reported in the Supporting Information.

The equilibrium between intramolecularly hydrogen-bonded and non-hydrogen-bonded states of the present series of PBIs was investigated by Fourier-transform infrared (FT-IR) spectroscopy at room temperature. It was previously reported that the intramolecularly hydrogen-bonded amide hydrogens of the monomeric **PBI-1-C2** in 1,1,2,2-tetrachloroethane (TCE) can be characterized by the appearance of a new N−H stretching frequency in the FT-IR spectrum at 3409 cm^{-1}, which is shifted to lower energy by 37 cm^{-1} in comparison with the $\tilde{\nu}$(N−H) bond (3446 cm^{-1}) of non-hydrogen-bonded amide hydrogens of **ref-C2**.[13] The signal at 3446 cm^{-1} becomes more dominant in the N−H stretching region with the increasing length of the alkyl spacer from ethylene (C2) to pentylene (C5) chain (Figure 2a). The influence of the spacer length on the equilibrium between hydrogen-bonded and non-hydrogen-bonded species is clearly visible in the plot of ratios of transmittance at 3446 to 3409 cm^{-1} (T_{3446}/T_{3409}) as a function of the spacer length (Figure 2b). Notably, the T_{3446}/T_{3409} values of **PBI-1-C5** are already comparable to that of non-hydrogen-bonding benzamide **ref-C2**, indicating that this PBI derivative exists mainly in non-hydrogen-bonded conformations in TCE. For **PBI-1-C4**, the percentage of hydrogen-bonded molecules appears to be also small in this more polar solvent although NMR data support the coexistence of hydrogen-bonded molecules in equilibrium with non-hydrogen-bonded ones (Supporting Information Figure S1 and Table S1). In solvents of lower polarity, hydrogen-bonding becomes stronger[18] and accordingly a larger fraction of molecules is expected to prevail in the intramolecularly hydrogen-bonded state. ^{1}H NMR spectra for the monomeric **PBI-1-C4** in less polar deuterated toluene indeed corroborate this view as the proton peaks of the amide and trialkoxyphenyl groups are significantly downfield-shifted compared with those of **ref-C2** due to the ring current effect of the PBI on protons in close vicinity for the intramolecularly hydrogen-bonded conformation (Supporting Information Figure S1 and Table S2).

To gain more insight into the molecular conformation of the monomeric states of the PBIs, their optical properties have been explored by UV/vis absorption and steady-state fluorescence spectroscopy in TCE under dilute conditions.

DOI: 10.1021/jacs.5b11674
J. Am. Chem. Soc. 2016, 138, 670−678

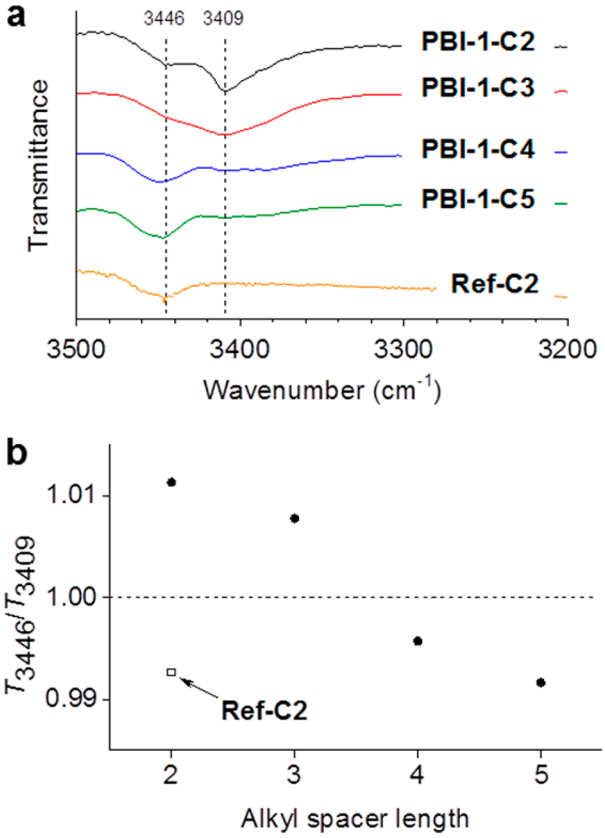

Figure 2. (a) N−H stretching regions of the FT-IR spectra of monomeric PBI derivatives and **ref-C2** in 1,1,2,2-tetrachloroethane (c_T = 0.5 × 10^{-3} M) at room temperature. (b) T_{3446}/T_{3409} ratios are plotted with respect to the length of the alkyl linkers.

The absorption spectra of the present PBI derivatives show the characteristic vibronic pattern for PBI monomers with absorption maxima at around 532 nm, and the spectral features of these PBIs in the monomeric state are independent of the spacer length. Likewise, the emission spectra of these PBIs exhibit common spectral features that are independent of spacer alkyl chain length (Figure 3a). Interestingly, however, they exhibit very different fluorescence quantum yields. Thus, **PBI-1-C2** and **PBI-1-C3** exhibit in TCE very low fluorescence quantum yields of 10% and 15%, respectively. This strong fluorescence quenching, compared with that of a phenyl-substituted PBI derivative without alkoxy groups (quantum yield is 65%),[19] can be attributed to a photoinduced intramolecular electron transfer from the electron-rich trialkoxyphenyl group to the electron-deficient PBI unit. The fluorescence quantum yield in the same solvent is drastically increased to 33% for **PBI-1-C4** and 58% for **PBI-1-C5**, clearly indicating a remarkable dependence on the spacer chain length. This enhanced emission, compared to that of C2 and C3 derivatives, may be explained based on inefficient intramolecular electron transfer due to an increased distance between the electron-donating trialkoxyphenyl group and electron-accepting PBI core.

In this regard, the efficiency of electron transfer and hence the fluorescence quantum yield of the present series of PBIs should be sensitively dependent on their monomer conformation directed by the intramolecular hydrogen bonds, which can be controlled by the choice of the solvent, i.e., its capacity to act as a hydrogen-bond donor or acceptor.

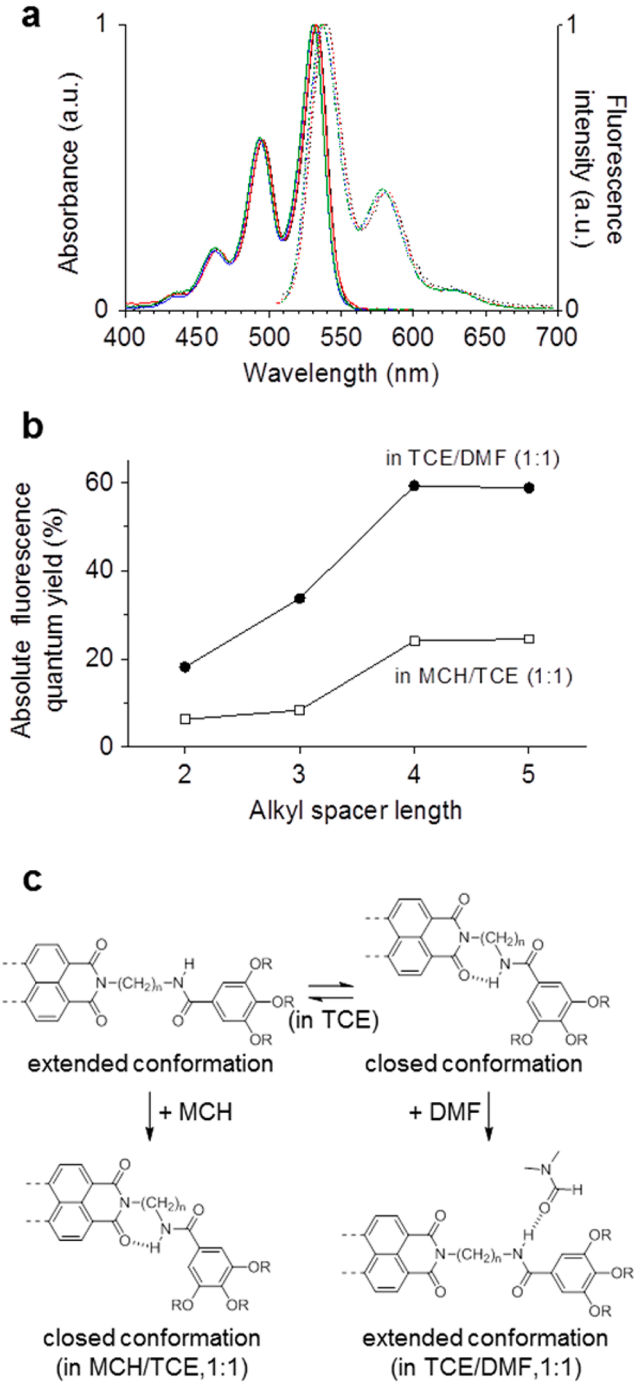

Figure 3. (a) Absorption (solid lines) and fluorescence spectra (dashed lines) of the monomeric **PBI-1-C2** (black), **PBI-1-C3** (red), **PBI-1-C4** (blue), and **PBI-1-C5** (green) in TCE at a concentration below 1 × 10^{-6} M. (b) Solvent-dependent fluorescence quantum yields of monomeric PBIs in MCH/TCE (1:1, v/v, open squares) and in TCE/DMF (1:1, v/v, closed circles). (c) Conceivable conformational changes in the monomeric state of PBIs upon addition of MCH or DMF to their TCE solutions. Only one-half of each of these symmetrical structures is shown, and the dodecyl groups are denoted as R.

Therefore, solvent-dependent fluorescence quantum yields of **PBI-1-C2** to **PBI-1-C5** were determined. Indeed, the fluorescence quantum yields of all these PBIs become higher in the presence of a polar hydrogen-bond acceptor cosolvent such as dimethylformamide (DMF), whereas they become

DOI: 10.1021/jacs.5b11674
J. Am. Chem. Soc. 2016, 138, 670−678

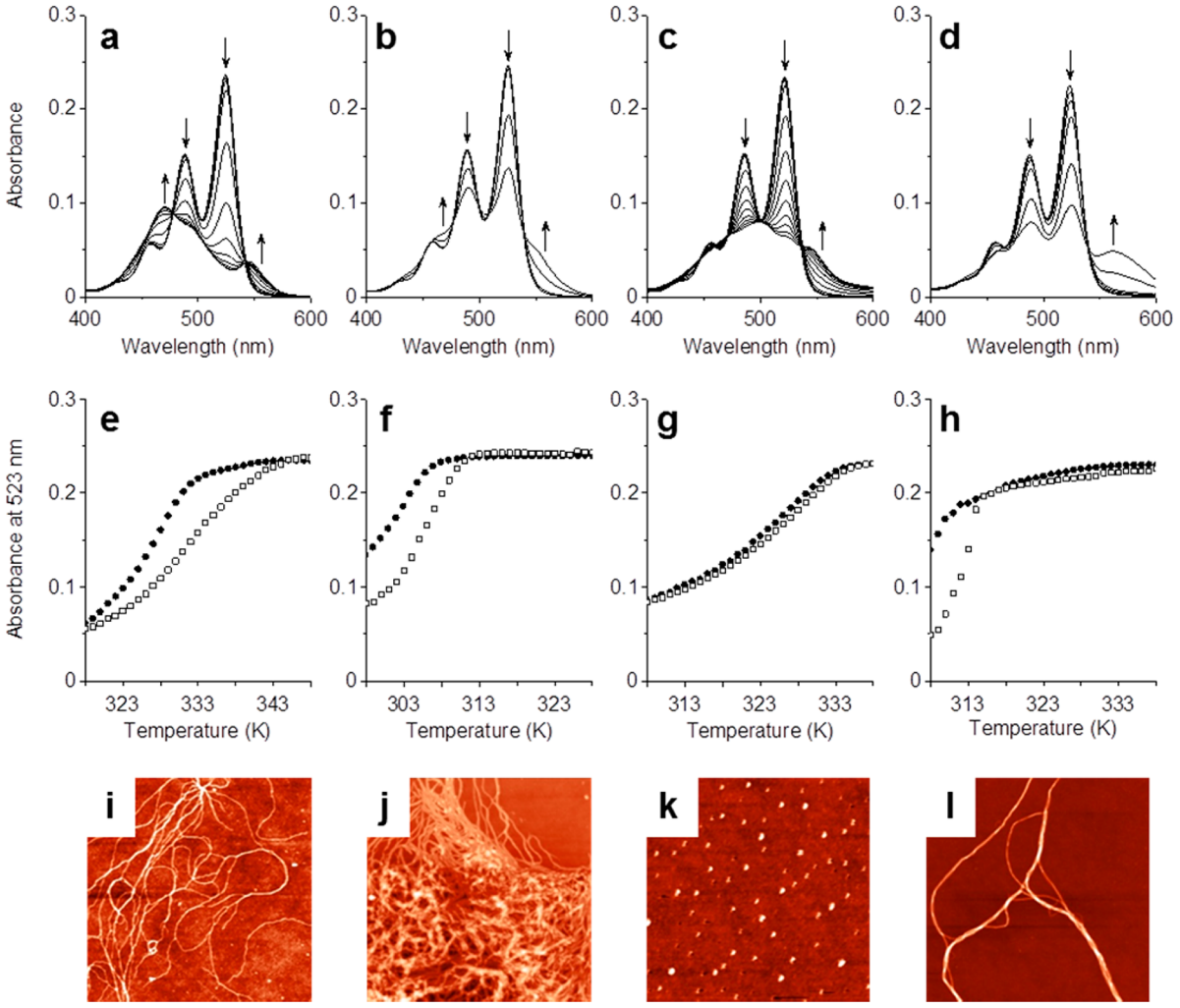

Figure 4. Temperature-dependent absorption spectral changes of (a) **PBI-1-C2**, (b) **PBI-1-C3**, (c) **PBI-1-C4**, and (d) **PBI-1-C5** observed during the cooling process at a rate of 1 K min^{-1}. Conditions: $c_T = 5 \times 10^{-6}$ M, MCH/toluene (2:1, v/v). Plots of absorbance at 523 nm of (e) **PBI-1-C2**, (f) **PBI-1-C3**, (g) **PBI-1-C4**, and (h) **PBI-1-C5** as a function of temperature observed during cooling processes at rates of 1 K min^{-1} (closed circles) and 0.1 K min^{-1} (open squares). AFM height images (5 μm × 5 μm) of (i) **PBI-1-C2**, (j) **PBI-1-C3**, (k) **PBI-1-C4**, and (l) **PBI-1-C5**, spin-coated (3000 rpm) onto silicon substrates from each aggregate solution. The structural details of the nanoparticles of **PBI-1-C4** (Figure 4k) are elucidated in more detail in the Supporting Information, Table S3.

lower in a presence of a nonpolar cosolvent such as methylcyclohexane (MCH) (Figure 3b). This solvent dependency of fluorescence properties is quite unusual, even contrary to the common perception for photoinduced electron transfer process, because the charge-separated state is usually better stabilized in more polar solvents, leading to a faster depopulation of the initial fluorescent state according to Marcus theory.[20]

An explanation for this unusual solvent dependency can be provided based on the solvent-dependent change of the molecular conformation, i.e., from an extended form in the hydrogen-bond-breaking solvent DMF to an intramolecularly hydrogen-bonded closed conformation in nonpolar MCH where hydrogen bonds become particularly strong (Figure 3c).[18] For such a situation, the distance between the donor and acceptor units of **PBI-1** becomes more significant for the kinetics of the photoinduced electron transfer process than the stabilization of the charge-separated state.[21] This interpretation corroborates our experimental findings that the PBIs with longer alkyl spacers (C4 and C5 chains) show the largest difference in fluorescence quantum yields in polar solvent TCE/DMF compared with those in nonpolar MCH/TCE, as the PBIs with longer alkyl spacers provide greater donor–acceptor distances for the extended conformations compared to those of the closed conformations. With regard to our subsequent self-assembly studies, it is important to point out that these fluorescence studies reveal that all the investigated PBI derivatives prevail in the intramolecularly hydrogen-bonded, closed conformation in nonpolar solvents (Figure 3c).

Supramolecular Polymerization. The kinetic stability of the intramolecularly hydrogen-bonded state of PBIs in the supramolecular polymerization process was investigated by temperature-dependent UV/vis spectroscopy at different cooling rates (Figure 4). As reported previously, **PBI-1-C2** self-assembles in MCH/toluene (2:1, v/v) into elongated one-dimensional nanofibers through a cooperative nucleation–growth process.[13] An important aspect in the supramolecular polymerization process is that the monomeric species are kinetically trapped in the intramolecularly hydrogen-bonded state upon cooling, and accordingly the spontaneous nucleation is temporarily retarded. The unique kinetics of the nucleated supramolecular polymerization was confirmed by a shift of the

DOI: 10.1021/jacs.5b11674
J. Am. Chem. Soc. 2016, 138, 670–678

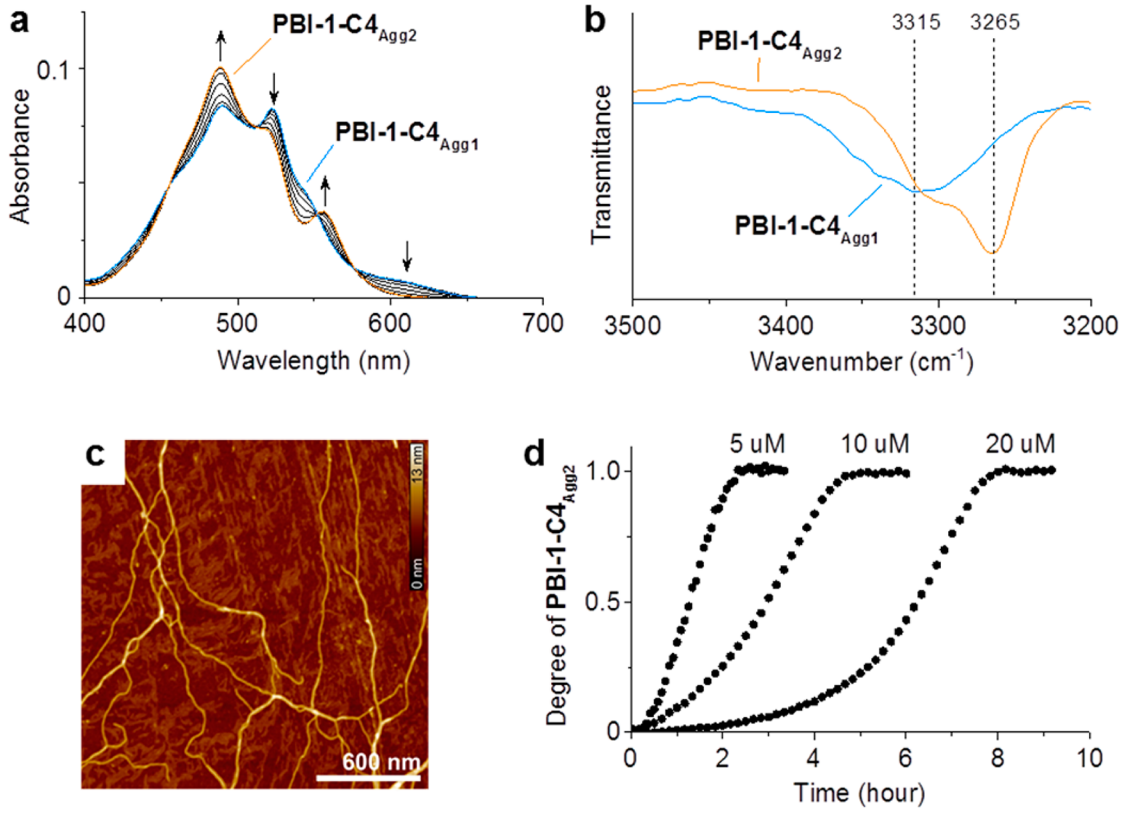

Figure 5. (a) Time-dependent (0 to 3 h) UV/vis absorption changes showing the transformation from **PBI-1-C4**$_{Agg1}$ to **PBI-1-C4**$_{Agg2}$ upon stirring. Condition: $c_T = 5 \times 10^{-6}$ M, MCH/toluene (2:1, v/v), 308 K, 400 rpm. The arrows indicate spectral changes with increasing time. (b) N−H stretching regions of FT-IR spectra for **PBI-1-C4**$_{Agg1}$ and **PBI-1-C4**$_{Agg2}$ solutions in MCH/toluene (2:1, v/v) at $c_T = 5 \times 10^{-4}$ M. (c) AFM height image of **PBI-1-C4**$_{Agg2}$, spin-coated (3000 rpm) onto silicon wafers from the MCH/toluene (2:1) solution. (d) Time-dependent degree of **PBI-1-C4**$_{Agg2}$ formation calculated from the apparent absorption coefficients at $\lambda = 488$ nm observed in the transformation process from **PBI-1-C4**$_{Agg1}$ to **PBI-1-C4**$_{Agg2}$ in MCH/toluene (2:1, v/v) at the given concentrations (indicated above the respective curve) and temperature of 308 K under stirring at a rate of 400 rpm.

critical temperature from 332 to 343 K as the cooling rate was decreased from 1 to 0.1 K min^{-1} (Figure 4e). Thus, the self-assembly behavior of the other PBI derivatives (**PBI-1-C3** to **PBI-1-C5**) was investigated in the same solvent MCH/toluene (2:1, v/v) by monitoring the temperature-dependent absorption changes at $\lambda = 523$ nm with different cooling rates (Figures 4f–h). Upon cooling at a rate of 1 K min^{-1}, the supramolecular polymerization proceeded abruptly at the critical temperature of 307 K for **PBI-1-C3** and 312 K for **PBI-1-C5** (Figures 4f,h, closed circles). These critical temperatures are increased by 4 and 3 K, respectively, with decreasing the cooling rate from 1 to 0.1 K min^{-1} (Figures 4f,h, open squares). The dependency of the critical temperature on cooling rate is indicative of the fact that the intramolecularly hydrogen-bonded species delay the spontaneous polymerizations of **PBI-1-C3** and **PBI-1-C5**. In contrast, for the self-assembly process of **PBI-1-C4**, no noticeable effect of cooling rate was observed, indicating the absence of a kinetic stabilization of the monomeric state (Figure 4g). Atomic force microscopy (AFM) images showed the formation of nanoparticles of **PBI-1-C4** in MCH/toluene (2:1, v/v) upon cooling, which distinctly differ from the fibrous structures observed from the aggregate solutions of the other PBI derivatives (Figures 4i–l). The unexpected insensitivity of nucleation on cooling rate and formation of nanoparticles suggest that **PBI-1-C4** follows a different self-assembly pathway compared to the earlier investigated **PBI-1-C2**[13] and the other two new derivatives **PBI-1-C3** and **PBI-1-C5**.

Computer-generated molecular models have provided valuable structural information for the different self-assembly behavior of **PBI-1-C4** compared to other investigated PBIs. Thus, structural models of **PBI-1-C4** reveal that the nine-membered ring of the intramolecular hydrogen-bonded trialkoxybenzamide group is located almost in the same plane as the PBI π-surface (Supporting Information Figure S2c). This is in contrast to the other PBI derivatives (Figures S2a,b,d) where the hydrogen bonding directs the trialkoxyphenyl groups out of the PBI plane up to an almost orthogonal orientation for **PBI-1-C2** and **PBI-1-C3**. Accordingly, while self-assembly by $\pi-\pi$ stacking becomes disfavored for **PBI-1-C2**, **PBI-1-C3**, and **PBI-1-C5** due to the hydrogen-bonded conformational preference leading to shielding of the π-faces, it becomes favored for the prevailing conformation of **PBI-1-C4**.

Moreover, the temperature-dependent absorption changes from the aggregate to monomeric state, i.e., upon heating follow a nonsigmoidal transition that could be fitted by using the cooperative growth model with $\Delta H_e = -58$ kJ mol^{-1} and $T_e = 335$ K at the given concentration of 5×10^{-6} M (Supporting Information Figure S3).[22] The lower value of ΔH_e by nearly half in comparison with that of **PBI-1-C2** ($\Delta H_e = -109$ kJ mol^{-1})[13] supports the assumption that intermolecular hydrogen-bonding interactions of amide groups are less involved in the self-assembly process of **PBI-1-C4** into nanoparticle-shaped aggregates.

DOI: 10.1021/jacs.5b11674
J. Am. Chem. Soc. 2016, 138, 670−678

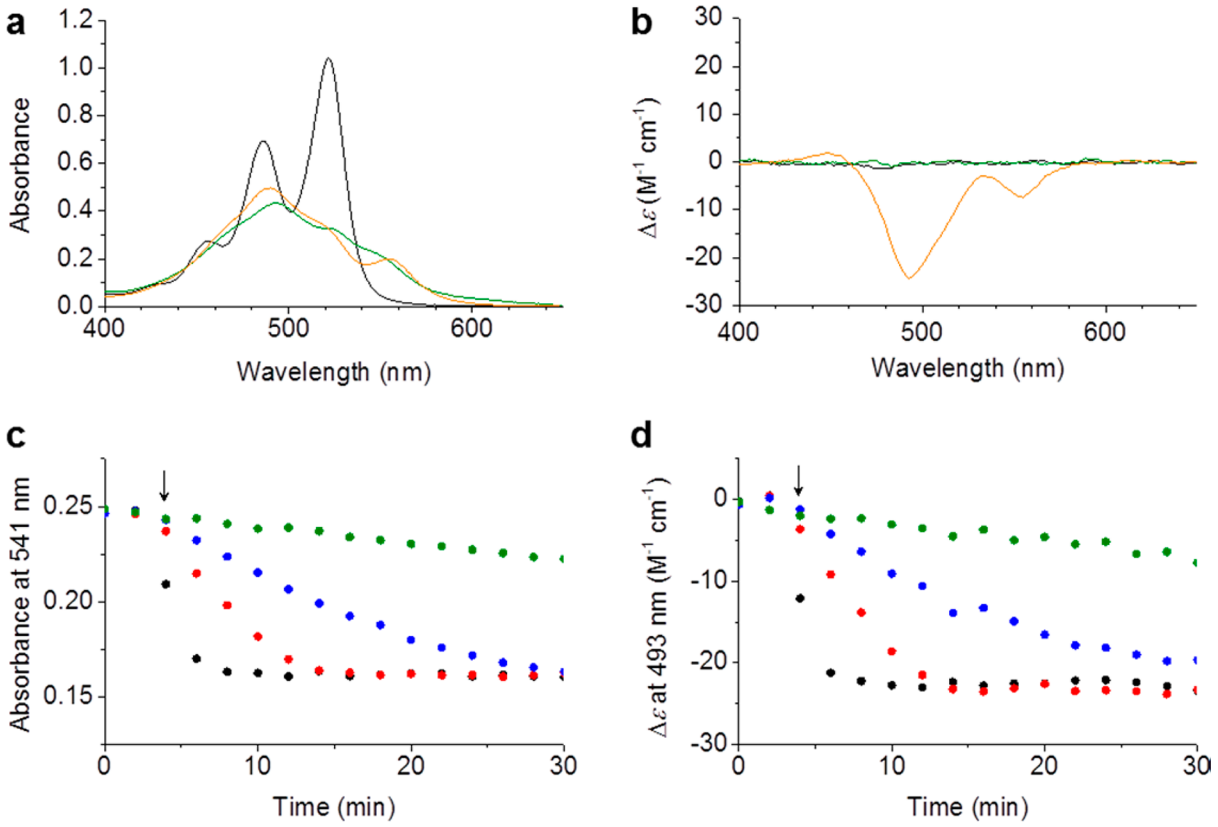

Figure 6. (a) Absorption and (b) CD spectra of the monomeric **PBI-1-C4** (black lines), and **PBI-1-C4**$_{Agg1}$ (green lines) and **PBI-1-C4**$_{Agg2}$ (orange lines) in (*S*)-limonene. Conditions: $c_T = 2 \times 10^{-5}$ M, 298 K for the aggregate samples, and 363 K for the monomer sample. (c, d) Plots of the changes in absorbance at 541 nm (c) and CD intensity at 493 nm (d) as a function of time after the sonicated solution of **PBI-1-C4**$_{Agg2}$ in (*S*)-limonene was added to the solution of **PBI-1-C4**$_{Agg1}$ in (*S*)-limonene at a certain time (indicated by arrows) under the conditions of [**PBI-1-C4**$_{Agg1}$]/[**PBI-1-C4**$_{Agg2}$] = 5 (black dots), 30 (red dots), 60 (blue dots), and 300 (green dots) at a temperature of 298 K.

The unexpected nanoparticle aggregate state of **PBI-1-C4** (**PBI-1-C4**$_{Agg1}$) is stable for several hours in MCH/toluene (2:1, v/v) at a concentration of 5×10^{-6} M and a temperature of 308 K (Supporting Information Figure S4). Interestingly, under stirring at a rate of 400 rpm, it transformed within 3 h into a different aggregate (**PBI-1-C4**$_{Agg2}$). This transformation is accompanied by the rearrangement of hydrogen bondings of amide groups and $\pi-\pi$ stacking of PBI molecules, as confirmed by FT-IR and UV/vis absorption spectral measurements (Figure 5a,b). The FT-IR spectrum of **PBI-1-C4**$_{Agg2}$ shows a new stretching frequency at 3265 cm^{-1} in the N−H stretch region, which is in agreement with the band observed for intermolecularly hydrogen-bonded amide hydrogens in a xerogel phase of **PBI-1-C2** ($\tilde{\nu}$(N−H) = 3271 cm^{-1}).[17a] AFM images revealed that the morphology changed as well from nanoparticles to nanofibers in the transition process from **PBI-1-C4**$_{Agg1}$ to **PBI-1-C4**$_{Agg2}$ (Figures 4k and 5c). The nanofibers **PBI-1-C4**$_{Agg2}$ was characterized by a mean height of 3.6 ± 0.2 nm, a length of several micrometers, and both left- and right-handed helices with the helical pitch of 11.5 ± 0.3 nm (Supporting Information Figure S5). The time-dependent absorption changes at 488 nm reveal a sigmoidal transition, which is characteristic of an autocatalytic process that consists of kinetically prevented nucleation, followed by accelerating growth processes (Figure 5d).[5,13,23] Importantly, the time at which the fibril formation reaches 50% completion becomes longer as the total concentration of **PBI-1-C4** increased (Figure 5d). This concentration dependence is opposed to the one observed for **PBI-1-C2**,[13] but resembles that of other reported systems in which the monomeric species are trapped in the form of thermodynamically disfavored aggregates.[5,24] The nanoparticles **PBI-1-C4**$_{Agg1}$ are such off-pathway aggregation products, which are thermodynamically unstable and eventually transform into the supramolecular polymers **PBI-1-C4**$_{Agg2}$ over time. Regarding the dissociation process from **PBI-1-C4**$_{Agg2}$ to monomeric state upon heating of the solution at the given concentration of 5×10^{-6} M, thermodynamic parameters $\Delta H_e = -112$ kJ mol^{-1} and $T_e = 332$ K were determined by fitting the temperature-dependent data to the cooperative model (Supporting Information Figure S6).[22] The significant decrease of the ΔH_e value compared with that for the formation of **PBI-1-C4**$_{Agg1}$ ($\Delta H_e = -58$ kJ mol^{-1}) indeed confirms that intermolecular hydrogen bonding of amide groups is not involved in the nanoparticle formation, but it is involved in the nanofiber-forming supramolecular polymerization process.

Impact of Chiral Solvents and Added Seeds. It is noteworthy that the transition from off-pathway aggregates **PBI-1-C4**$_{Agg1}$ into supramolecular polymers **PBI-1-C4**$_{Agg2}$ could be confirmed also in pure nonpolar solvents such as (*S*)-limonene (Figure 6a). The chiral solvents (*R*)- and (*S*)-limonene were used in our earlier studies to bias the self-assembly of the achiral **PBI-1-C2** into single-handed helical fibers with an enantiomeric excess close to 100%.[17b,c] Interestingly, the circular dichroism (CD) spectroscopic study on the self-assembly of **PBI-1-C4** in (*S*)-limonene revealed that **PBI-1-C4**$_{Agg1}$ is CD silent, while **PBI-1-C4**$_{Agg2}$ showed a strong Cotton effect (Figure 6b). These results indicate that the chiral solvent (*S*)-limonene does not exert a chiral bias on the less

DOI: 10.1021/jacs.5b11674
J. Am. Chem. Soc. 2016, 138, 670−678

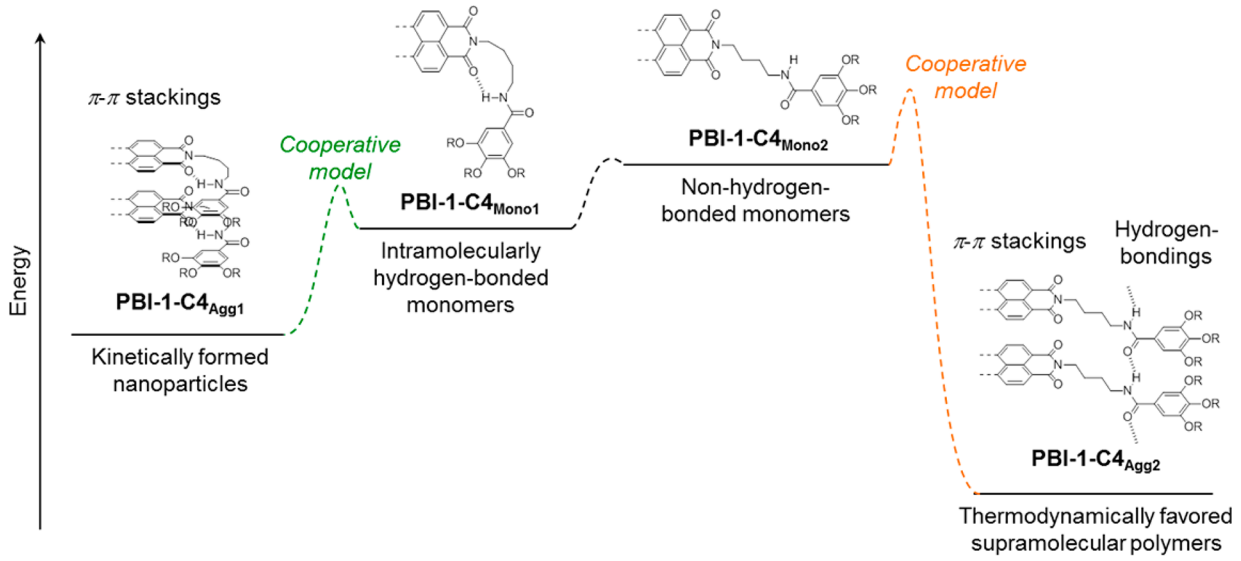

Figure 7. Qualitative energy landscape of two competing aggregation pathways of **PBI-1-C4** illustrated on the basis of the thermodynamic parameters determined by cooperative supramolecular polymerization models. For simplicity, one-half of each structure is shown and the dodecyl groups are replaced by R.

defined nanoparticle **PBI-1-C4**$_{Agg1}$ aggregates but impacts the packing arrangement of PBI molecules in **PBI-1-C4**$_{Agg2}$, leading to helical fibrous aggregates, where intermolecular hydrogen bonds between amide groups are involved.

Like in MCH/toluene also in (*S*)-limonene under stirring at a rate of 400 rpm at a temperature of 298 K, the initially formed off-pathway aggregates **PBI-1-C4**$_{Agg1}$ transformed slowly into **PBI-1-C4**$_{Agg2}$ (Supporting Information Figure S7). This kinetic profile changed dramatically upon addition of a sonicated solution of **PBI-1-C4**$_{Agg2}$ into the solution of off-pathway aggregates **PBI-1-C4**$_{Agg1}$ in (*S*)-limonene. Both time-dependent UV/vis and CD spectroscopic studies confirm the successful seeded polymerization, where the transformation from **PBI-1-C4**$_{Agg1}$ to **PBI-1-C4**$_{Agg2}$ was initiated without a lag time, and the transformation kinetics was controllable with different amount of externally added **PBI-1-C4**$_{Agg2}$ seeds (Figures 6c,d).

Mechanism of Supramolecular Polymerization. Taking into account our thermodynamic and kinetic data on the self-assembly behavior of **PBI-1-C4**, we propose an energy landscape consisting of two aggregation pathways that lead either to the formation of kinetically favored nanoparticles or thermodynamically favored supramolecular fibers (Figure 7). The unprecedented feature of this system is that both pathways proceed in cooperative nucleation-growth processes that originate from different molecular conformations in the monomeric state. Namely, nanoparticle-shaped **PBI-1-C4**$_{Agg1}$ originates from the self-assembly of energetically favored intramolecularly hydrogen-bonded monomers (**PBI-1-C4**$_{Mono1}$), while fibrous **PBI-1-C4**$_{Agg2}$ is obtained from the self-assembly of monomers which prevail in the energetically less favored non-hydrogen-bonded open conformation (**PBI-1-C4**$_{Mono2}$). The former aggregation process was not observed for the previously investigated **PBI-1-C2** with the shorter ethylene spacer but has now been successfully realized by introducing the longer butylene linker between the amide and imide groups in **PBI-1-C4** whose different conformation allowed the formation of π-stacked PBIs in the intramolecularly hydrogen-bonded state (Supporting Information Figure S2). As a consequence of the accumulation of **PBI-1-C4** in the off-pathway aggregate state, the nucleated supramolecular polymerization into the thermodynamically more stable **PBI-1-C4**$_{Agg2}$ becomes kinetically severely delayed because in addition to the energy barrier provided by the formation of intramolecularly hydrogen-bonded **PBI-1-C4**$_{Mono1}$ the majority of these monomers are now accumulated in energetically more stable off-pathway self-assembly product **PBI-1-C4**$_{Agg1}$. Nevertheless, the addition of sonicated **PBI-1-C4**$_{Agg2}$ into the off-pathway **PBI-1-C4**$_{Agg1}$ initiates the transformation from **PBI-1-C4**$_{Agg1}$ into **PBI-1-C4**$_{Agg2}$ without a lag time. Accordingly, **PBI-1-C4**$_{Agg2}$ seeds can catalyze the transformation into the thermodynamically more stable supramolecular polymer (Figure 7).

Regarding the kinetic stability of trapped states, for **PBI-1-C2** the dilute conditions extended the lag time for the transformation from intramolecularly hydrogen-bonded monomers into supramolecular polymers. In contrast, for the off-pathway aggregate **PBI-1-C4**$_{Agg1}$ an increase of the kinetic stability was observed at higher concentrations (Figure 5d). These results, which are well explained by the presence or absence of an additional off-pathway state (Figure 7), have indeed significant impact also on macroscopic gelation properties and explain why organogelator design is still a challenging task.[25,26] Thus, scanning electron microscopy (SEM) images showed that **PBI-1-C4** in cyclohexane at the high concentration of 1×10^{-3} M prevails in its nanoparticle state even 1 day at ambient temperature (Figure 8a). This observation is in strong contrast to the observations made for the cyclohexane solutions of many other PBI derivatives, including **PBI-1-C2**, **PBI-1-C3**, and **PBI-1-C5**, that instantaneously or at least within a few hours form fibrous nanostructures upon cooling, leading to gelation of nonpolar solvent cyclohexane (Supporting Information Figure S9). However, as it is the case under dilute conditions in MCH/toluene (Figures 4k and 5c), the concentrated solution of **PBI-1-C4** in cyclohexane nanoparticles can transform into fibrous nanostructures, giving a transparent gel after 5 days (Figure 8b, Supporting Information Figure S10). Such a long kinetics in the gelation process paves the way for the development of a seed-induced gelation methodology, which

DOI: 10.1021/jacs.5b11674
J. Am. Chem. Soc. 2016, 138, 670−678

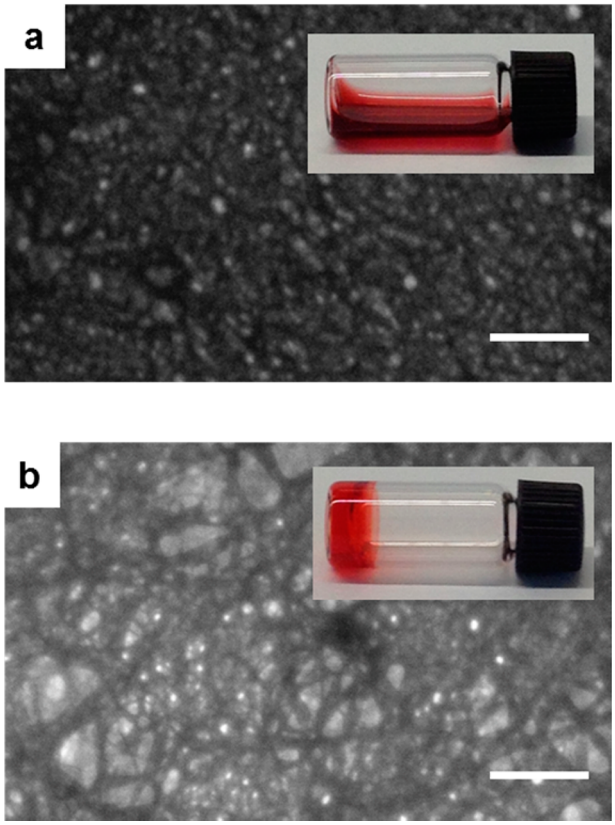

Figure 8. SEM images of the nanoparticle-shaped **PBI-1-C4**$_{Agg1}$ (a) and fibrous **PBI-1-C4**$_{Agg2}$ (b) drop-casted on a silicon wafer from a cyclohexane solution (c_T = 1 × 10^{-3} M) obtained 1 day and 5 days after cooling to room temperature, respectively. Scale bar, 1 μm. Inserts: Photographs of **PBI-1-C4**$_{Agg1}$ solution and **PBI-1-C4**$_{Agg2}$ gel. Detailed information about the morphological parameters of **PBI-1-C4**$_{Agg1}$ and **PBI-1-C4**$_{Agg2}$ are shown in Supporting Information Figure S8 and Table S3.

is applicable to the micro/nanoscale engineering of materials consisting of fiber networks.[27]

CONCLUSION

We have investigated the impact of alkyl spacer lengths between amide and imide groups on the kinetic stability of the intramolecularly hydrogen-bonded PBI monomers and supramolecular polymerization process by employing a series of PBIs with varied spacer lengths. While propylene- and pentylene-tethered PBI derivatives followed the previously reported supramolecular polymerization mechanism for the ethylene-tethered PBI, detailed spectroscopic and microscopic studies revealed a quite distinct self-assembly behavior for the butylene-tethered PBI. In this case, intramolecularly hydrogen-bonded PBI monomers spontaneously self-assemble into nanoparticles, which transform only slowly into fibrous supramolecular polymers over time. Kinetic and thermodynamic analyses allowed us to conclude that the nanoparticles constitute an off-pathway aggregate state with regard to the thermodynamically stable fibrous supramolecular polymers. On the basis of these findings, we have proposed an energy landscape of two competing aggregation pathways. Importantly, both pathways can be described by the cooperative nucleation-elongation model but are directed from two different monomeric species. Namely, intramolecularly hydrogen-bonded monomers form the off-pathway nanoparticle, while the self-assembly into fibrous supramolecular polymers requires monomers in the energetically less favored non-hydrogen-bonded open conformation. Because of a large energy barrier provided by the formation of the off-pathway nanoparticle, the spontaneous supramolecular polymerization becomes efficiently inhibited in the lowest polarity solvents at higher concentrations. This enables long-time stable fluid dispersions despite their far-from-equilibrium nature which can, however, be transformed at any time by performing the seed-induced living supramolecular polymerization.

ASSOCIATED CONTENT

Supporting Information

The Supporting Information is available free of charge on the ACS Publications website at DOI: 10.1021/jacs.5b11674.

Synthesis and characterization of PBI derivatives, energy minimized structures of intramolecularly hydrogen-bonded PBI monomers, and AFM and SEM studies on PBI aggregate samples (PDF)

AUTHOR INFORMATION

Corresponding Author

*wuerthner@chemie.uni-wuerzburg.de

Notes

The authors declare no competing financial interest.

ACKNOWLEDGMENTS

S.O. thanks the JSPS Postdoctoral Fellowship for Research Abroad for financial support. Financial support by the Bavarian State Ministry of Science, Research, and the Arts for the Center for Nanosystems Chemistry, is gratefully acknowledged.

REFERENCES

(1) (a) Yang, L.; Tan, X.; Wang, Z.; Zhang, X. *Chem. Rev.* **2015**, *115*, 7196−7239. (b) Rest, C.; Kandanelli, R.; Fernández, G. *Chem. Soc. Rev.* **2015**, *44*, 2543−2572.

(2) (a) Würthner, F. *Nat. Chem.* **2014**, *6*, 171−173. (b) Van der Zwaag, D.; De Greef, T. F. A.; Meijer, E. W. *Angew. Chem., Int. Ed.* **2015**, *54*, 8334−8336. (c) Mukhopadhyay, R. D.; Ajayaghosh, A. *Science* **2015**, *349*, 241−242.

(3) (a) Tidhar, Y.; Weissman, H.; Wolf, S. G.; Gulino, A.; Rybtchinski, B. *Chem. - Eur. J.* **2011**, *17*, 6068−6075. (b) Rybtchinski, B. *ACS Nano* **2011**, *5*, 6791−6818. (c) Rosen, B. M.; Peterca, M.; Morimitsu, K.; Dulcey, A. E.; Leowanawat, P.; Resmerita, A.-M.; Imam, M. R.; Percec, V. *J. Am. Chem. Soc.* **2011**, *133*, 5135−5151. (d) Roche, C.; Sun, H.-J.; Prendergast, M. E.; Leowanawat, P.; Partridge, B. E.; Heiney, P. A.; Araoka, F.; Graf, R.; Spiess, H. W.; Zeng, X.; Ungar, G.; Percec, V. *J. Am. Chem. Soc.* **2014**, *136*, 7169−7185. (e) Korevaar, P. A.; Newcomb, C. J.; Meijer, E. W.; Stupp, S. I. *J. Am. Chem. Soc.* **2014**, *136*, 8540−8543.

(4) De Greef, T. F. A.; Smulders, M. M. J.; Wolffs, M.; Schenning, A. P. H. J.; Sijbesma, R. P.; Meijer, E. W. *Chem. Rev.* **2009**, *109*, 5687−5754.

(5) Ogi, S.; Sugiyasu, K.; Manna, S.; Samitsu, S.; Takeuchi, M. *Nat. Chem.* **2014**, *6*, 188−195.

(6) (a) Wang, X.; Guerin, G.; Wang, H.; Wang, Y.; Manners, I.; Winnik, M. A. *Science* **2007**, *317*, 644−647. (b) Gilroy, J. B.; Gädt, T.; Whittell, G. R.; Chabanne, L.; Mitchels, J. M.; Richardson, R. M.; Winnik, M. A.; Manners, I. *Nat. Chem.* **2010**, *2*, 566−570. (c) Patra, S. K.; Ahmed, R.; Whittell, G. R.; Lunn, D. J.; Dunphy, E. L.; Winnik, M. A.; Manners, I. *J. Am. Chem. Soc.* **2011**, *133*, 8842−8845. (d) Robinson, M. E.; Lunn, D. J.; Nazemi, A.; Whittell, G. R.; De Cola, L.; Manners, I. *Chem. Commun.* **2015**, *51*, 15921−15924.

DOI: 10.1021/jacs.5b11674
J. Am. Chem. Soc. 2016, 138, 670−678

(7) Pal, A.; Malakoutikhah, M.; Leonetti, G.; Tezcan, M.; Colomb-Delsuc, M.; Nguyen, V. D.; van der Gucht, J.; Otto, S. *Angew. Chem., Int. Ed.* **2015**, *54*, 7852−7856.
(8) (a) Kasai, M.; Asakura, S.; Oosawa, F. *Biochim. Biophys. Acta* **1962**, *57*, 22−31. (b) Asakura, S.; Eguchi, G.; Iino, T. *J. Mol. Biol.* **1964**, *10*, 42−56.
(9) Zhao, D.; Moore, J. S. *Org. Biomol. Chem.* **2003**, *1*, 3471−3491.
(10) (a) Zhang, W.; Jin, W.; Fukushima, T.; Saeki, A.; Seki, S.; Aida, T. *Science* **2011**, *334*, 340−343. (b) Zhang, W.; Jin, W.; Fukushima, T.; Mori, T.; Aida, T. *J. Am. Chem. Soc.* **2015**, *137*, 13792−13795.
(11) Mattia, E.; Otto, S. *Nat. Nanotechnol.* **2015**, *10*, 111−119.
(12) (a) Kang, J.; Miyajima, D.; Itoh, Y.; Mori, T.; Tanaka, H.; Yamauchi, M.; Inoue, Y.; Harada, S.; Aida, T. *J. Am. Chem. Soc.* **2014**, *136*, 10640−10644. (b) Kang, J.; Miyajima, D.; Mori, T.; Inoue, Y.; Itoh, Y.; Aida, T. *Science* **2015**, *347*, 646−651.
(13) Ogi, S.; Stepanenko, V.; Sugiyasu, K.; Takeuchi, M.; Würthner, F. *J. Am. Chem. Soc.* **2015**, *137*, 3300−3307.
(14) Gellman, S. H.; Dado, G. P.; Liang, G.-B.; Adams, B. R. *J. Am. Chem. Soc.* **1991**, *113*, 1164−1173.
(15) Nowick, J. S.; Abdi, M.; Bellamo, A.; Love, J. A.; Martinez, E. J.; Noronha, G.; Smith, E. M.; Ziller, J. W. *J. Am. Chem. Soc.* **1995**, *117*, 89−99.
(16) (a) Baldwin, R. L. *Folding Des.* **1996**, *1*, R1−R8. (b) van der Zwaag, D.; Pieters, P. A.; Korevaar, P. A.; Markvoort, A. J.; Spiering, A. J. H.; de Greef, T. F. A.; Meijer, E. W. *J. Am. Chem. Soc.* **2015**, *137*, 12677−12688.
(17) (a) Li, X.-Q.; Stepanenko, V.; Chen, Z.; Prins, P.; Siebbeles, L. D. A.; Würthner, F. *Chem. Commun.* **2006**, 3871−3873. (b) Ghosh, S.; Li, X.-Q.; Stepanenko, V.; Würthner, F. *Chem. - Eur. J.* **2008**, *14*, 11343−11357. (c) Stepanenko, V.; Li, X.-Q.; Gershberg, J.; Würthner, F. *Chem. - Eur. J.* **2013**, *19*, 4176−4183.
(18) Würthner, F.; Thalacker, C.; Sautter, A.; Schärtl, W.; Ibach, W.; Hollricher, O. *Chem. - Eur. J.* **2000**, *6*, 3871−3886.
(19) (a) Würthner, F.; Thalacker, C.; Diele, S.; Tschierske, C. *Chem. - Eur. J.* **2001**, *7*, 2245−2253. (b) Würthner, F.; Chen, Z.; Dehm, V.; Stepanenko, V. *Chem. Commun.* **2006**, 1188−1190.
(20) Marcus, R. A. *Angew. Chem., Int. Ed. Engl.* **1993**, *32*, 1111−1222.
(21) (a) Polese, A.; Mondini, S.; Bianco, A.; Toniolo, C.; Scorrano, G.; Guldi, D. M.; Maggini, M. *J. Am. Chem. Soc.* **1999**, *121*, 3446−3452. (b) Sisido, M.; Hoshino, S.; Kusano, H.; Kuragaki, M.; Makino, M.; Sasaki, H.; Smith, T. A.; Ghiggino, K. P. *J. Phys. Chem. B* **2001**, *105*, 10407−10415.
(22) (a) Jonkheijm, P.; van der Schoot, P.; Schenning, A. P. H. J.; Meijer, E. W. *Science* **2006**, *313*, 80−83. (b) Smulders, M. M. J.; Schenning, A. P. H. J.; Meijer, E. W. *J. Am. Chem. Soc.* **2008**, *130*, 606−611. (c) Smulders, M. M. J.; Nieuwenhuizen, M. M. L.; de Greef, T. F. A.; van der Schoot, P.; Schenning, A. P. H. J.; Meijer, E. W. *Chem. - Eur. J.* **2010**, *16*, 362−367.
(23) (a) Bachmann, P. A.; Luisi, P. L.; Lang, J. *Nature* **1992**, *357*, 57−59. (b) Lohr, A.; Würthner, F. *Angew. Chem., Int. Ed.* **2008**, *47*, 1232−1236. (c) Carnall, J. M. A.; Waudby, C. A.; Belenguer, A. M.; Stuart, M. C. A.; Peyralans, J. J.-P.; Otto, S. *Science* **2010**, *327*, 1502−1506. (d) Baram, J.; Weissman, H.; Rybtchinski. *J. Phys. Chem. B* **2014**, *118*, 12068−12073.
(24) (a) Cui, H. G.; Chen, Z. Y.; Zhong, S.; Wooley, K. L.; Pochan, D. J. *Science* **2007**, *317*, 647−650. (b) Korevaar, P. A.; George, S. J.; Markvoort, A. J.; Smulders, M. M. J.; Hilbers, P. A. J.; Schenning, A. P. H. J.; De Greef, T. F. A.; Meijer, E. W. *Nature* **2012**, *481*, 492−496.
(25) Babu, S. S.; Praveen, V. K.; Ajayaghosh, A. *Chem. Rev.* **2014**, *114*, 1973−2129.
(26) Molla, M. R.; Ghosh, S. *Chem. Mater.* **2011**, *23*, 95−105.
(27) Li, J.-L.; Liu, X.-Y. *Adv. Funct. Mater.* **2010**, *20*, 3196−3216.

DOI: 10.1021/jacs.5b11674
J. Am. Chem. Soc. 2016, 138, 670−678